agronomy

MDPI

Article

Kernel Dehydration Characteristics Is Related to Kernel Microstructure and Starch Granule Size Distribution in Different Maize Varieties

Xuejie Li, Fengxue Suo, Zengxu Li, Yang Yang, Xin Hao, Qing Sun, Wen Jiang, Letian Liu, Ziyue Wang, Zeqian Shi, Jiushuo Li and Xuefang Sun *

College of Agronomy, Qingdao Agricultural University, Qingdao 266109, China; lixuejie1126@163.com (X.L.); 19105425851@163.com (F.S.); li2023x@163.com (Z.L.); 15847624520@163.com (Y.Y.); 17538221838@163.com (X.H.); sunqing0208@126.com (Q.S.); jwen1018@163.com (W.J.); 15634549648@163.com (L.L.); 19560729772@163.com (Z.W.); 13884698518@163.com (Z.S.); 15266452105@163.com (J.L.)
* Correspondence: sunxuefang@qau.edu.cn

Abstract

In the Huang-Huai-Hai region, a high kernel moisture content remains a primary constraint for the mechanical harvesting of maize kernels. Recent studies have largely focused on the relationships among ear traits, meteorological factors, and kernel dehydration. However, the regulatory mechanisms underlying the influence of kernel microstructure and starch granule size distribution on dehydration characteristics remain unclear. In this study, the fast-dehydrating variety Jingnongke 728 (JNK728) and the slow-dehydrating variety Zhengdan 958 (ZD958) were selected as experimental materials to compare the varietal differences in kernel microstructure and starch granule size distribution, and to investigate their roles in regulating kernel dehydration characteristics. The results showed that JNK728 had a significantly higher kernel dehydration rate (KDR). Compared with ZD958, JNK728 exhibited average increases of 15.22% in the pre-physiological maturity dehydration rate (pre-KDR) and 97.72% in the post-physiological maturity dehydration rate (post-KDR). The higher accumulations of kernel total starch content and amylopectin content were also observed in JNK728. Kernels of JNK728 were characterized by thinner pericarp at 35 days after pollination (DAP), lower vitreousness and a higher proportion of floury endosperm. Additionally, JNK728 displayed more uniformly sized starch granules with smooth surfaces, wider intergranular spaces, and looser starch packing. Moreover, the volume, number, and surface area of large starch granules (≥10 μm) in JNK728, increased by 2.91%, 10.94%, and 4.95%, respectively. These findings enhance the understanding of the regulatory role of kernel microstructure and starch granule size distribution in dehydration characteristics, offering theoretical guidance for the development of mechanical maize kernel harvesting technologies in the Huang-Huai-Hai region.

Keywords: maize; dehydration rate; starch content; endosperm structure; starch granules

check for updates

Received: 26 September 2025
Revised: 14 October 2025
Accepted: 22 October 2025
Published: 24 October 2025

Citation: Li, X.; Suo, F.; Li, Z.; Yang, Y.; Hao, X.; Sun, Q.; Jiang, W.; Liu, L.; Wang, Z.; Shi, Z.; et al. Kernel Dehydration Characteristics Is Related to Kernel Microstructure and Starch Granule Size Distribution in Different Maize Varieties. *Agronomy* **2025**, *15*, 2471. https://doi.org/10.3390/agronomy15112471

Copyright: © 2025 by the authors. Licensee MDPI, Basel, Switzerland. This article is an open access article distributed under the terms and conditions of the Creative Commons Attribution (CC BY) license (https://creativecommons.org/licenses/by/4.0/).

1. Introduction

Maize (*Zea mays* L.) is a major crop in China, serving as a crucial source of food, animal feed, and energy [1], and currently represents the highest yielding cereal crop worldwide [2]. Despite its importance, the mechanized harvesting rate of maize in China remains significantly lower than those of wheat and rice. The predominant harvesting methods include ear mechanical harvesting and manual harvesting [3,4], both of which

involve intermediate steps such as ear transportation, drying, and threshing [5]. In contrast, mechanical grain harvesting has been shown to reduce harvesting costs and improve production efficiency [6]. However, this technology has not yet reached maturity. According to recent reports, the adoption rate of maize mechanical grain harvesting remains below 5%, with a highly uneven regional distribution mainly concentrated in Xinjiang, Heilongjiang, and parts of northeastern Inner Mongolia [7].

The mechanized kernel harvest of maize is gaining increasing importance in China [8]. However, high kernel moisture content at harvest remains a major constraint [9,10] because it significantly increases the rates of kernel damage, postharvest losses, and impurities [11]. Excessive moisture necessitates post-harvest drying prior to transport and storage, thereby reducing grain quality, limiting the adoption of mechanical grain harvesting, and substantially lowering farmer income [5,12,13]. Therefore, achieving low kernel moisture content at harvest is critical for ensuring safe production, efficient transport, and reliable storage. In China, the optimal grain moisture content for mechanical grain harvesting ranges from 15% to 25% [14,15], with the lowest grain breakage rate occurring between 18% and 23% [16]. However, under traditional farming practices, maize kernels are typically harvested at a moisture content of approximately 30% after physiological maturity [17].

Kernel moisture content at physiological maturity, along with the average dehydration rates before and after physiological maturity, can directly influence moisture levels at harvest [18–20]. In this study, Zhengdan958 (ZD958) as a slow-dehydrating variety and Jingnongke (JNK728) as a fast-dehydrating variety were selected through the cluster analysis of 10 widely cultivated maize varieties based on kernel dehydration characteristics, growth period, and yield performance. A detailed investigation of the physiological mechanisms underlying the differences in kernel dehydration between these two varieties is expected to provide valuable insights for breeding and improving maize cultivars suitable for grain harvesting. These findings are of practical significance for advancing mechanical grain harvesting technology and promoting agricultural mechanization in China.

The dehydration characteristics of maize kernels are primarily determined by genotype and environmental conditions [21,22]. Previous studies have demonstrated that bract thickness, moisture content, and senescence rate are positively correlated with kernel dehydration rate [23,24]. Varieties exhibiting rapid dehydration of bracts and cobs tend to show faster kernel moisture loss [25]. In addition, shorter bracts and petioles along with greater pericarp permeability have been shown to promote kernel dehydration [26]. After physiological maturity, kernel dehydration is further influenced by ear traits such as ear axis diameter, number of ear rows, and overall ear maturity. Fewer ear rows are associated with faster dehydration, whereas thicker ear axes and larger ear sizes are considered less favorable for moisture reduction [27]. Although numerous studies have explored the relationships between ear morphology, meteorological conditions, and kernel dehydration under mechanical grain harvesting scenarios [10,28,29], limited attention has been paid to the role of internal kernel microstructure in regulating dehydration dynamics.

Grain type and internal structure have been shown to influence the dehydration of maize kernels [30,31]. A maize kernel consists of a pericarp, embryo, and endosperm [32]. Pericarp thickness is closely associated with the dehydration rate, with thicker pericarps typically resulting in slower moisture loss [33]. In addition to anatomical features, the internal structural and chemical composition of the kernel also affects dynamic dehydration. As the primary component of the kernel, starch plays a key role in determining both yield and quality. It exists in the form of starch granules, whose shape and size vary across varieties [34,35]. Maize endosperm can be classified into vitreous and floury types [36,37]. The compactness of protein and starch granules within the endosperm determines their structural organization and physicochemical properties. In the floury endosperm, starch

granules are loosely associated with a small amount of protein matrix and are predominantly spherical. In contrast, vitreous endosperm is characterized by dense binding of starch granules with protein and colloidal carbohydrates, where the granules are mostly small and spherical or large and polygonal in shape [38–40].

The arrangement, size, and number of starch granules reflect differences in the endosperm microstructure. However, the regulatory mechanisms by which starch granule volume, number, surface area, and structural characteristics within the endosperm influence kernel dehydration during mechanical grain harvesting remain unclear. In this study, the relationships between kernel dehydration and kernel starch microstructure were investigated, including kernel moisture content, weight of structural components, starch morphology, and starch granule characteristics. The objective was to clarify the role of kernel microstructure in regulating kernel dehydration rate (KDR), thereby providing theoretical support for the selection and breeding of maize varieties suitable for mechanical grain harvesting.

2. Materials and Methods

2.1. Site Description

The experiment was conducted from June to November in 2022 and 2023 in Jiangshan Town, Laixi City, Qingdao, Shandong Province (36°67′ N, 120°52′ E), China. The site is situated in a temperate semi-humid monsoon climate zone characterized by distinct dry and wet seasons, with rainfall typically coinciding with high temperatures. The soil at the experimental site was classified as a typical mortar black soil with a pH of 5.6. The physicochemical properties of the top 20 cm of soil were as follows: organic matter, 11.26 g kg^{-1}; alkali-hydrolyzable nitrogen, 88.26 mg kg^{-1}; total nitrogen, 0.81 g kg^{-1}; available phosphorus, 51.14 mg kg^{-1}; and available potassium, 132.13 mg kg^{-1}.

Meteorological data on temperature and precipitation during the two maize growing seasons are presented in Table 1. The average temperatures from June to November were 19.9 °C in 2022 and 20.4 °C in 2023. The total precipitation during the same period was 414.9 mm in 2022 and 209.2 mm in 2023, with the precipitation in 2022 being 98.32% higher than that in 2023.

Table 1. Average daily temperature and precipitation during maize growth period.

Month	2022		2023	
	Daily Average Temperature (°C)	Precipitation (mm)	Daily Average Temperature (°C)	Precipitation (mm)
June	23.4	80.9	23.8	28
July	26.5	54	27.4	23.8
August	25.3	176.8	25.7	141.8
September	20.5	66.5	21.9	13.1
October	13.4	27.8	16.3	0
November	10.3	8.9	7.3	2.5

2.2. Experiment Design and Plant Material

Two varieties with different kernel dehydration rates were used in this experiment. ZD 958 is a slow-dehydration variety, with Zheng 58 as its female parent and Chang 7-2 as its male parent; JNK728 is a fast-dehydration variety, with Jing MC01 as its female parent and Jing 2416 as its male parent. A randomized block design with three replicates was employed. Seeds were sown on 21 June 2022, and 22 June 2023, at a planting density of 67,500 plants ha^{-1} in plots measuring 540 m^2 each. The rows were spaced equally at 0.6 m intervals. Fertilization was applied as a basal treatment using a compound fertilizer

(N-P_2O_5-K_2O = 25-6-9) at a rate of 750 kg ha^{-1}. Table 2 summarizes the growth stages and accumulated temperatures of each variety from sowing to the final harvest for both growing seasons. Other field management practices were implemented in accordance with the standard high-yield maize cultivation protocols.

Table 2. Growth process and accumulated temperature of each variety.

Years	Hybrids	Sowing Dates	Silking	Physiological Maturity	Harvest	Accumulated Temperature from Sowing to Pollination	Accumulated Temperature from Pollination to Physiological Maturity	Accumulated Temperature from Physiological Maturity to Harvest
		(M-D)	(M-D)	(M-D)	(M-D)	(°C·d)	(°C·d)	(°C·d)
2022	ZD958	6-21	8-15	10-27	11-02	1471.8	1351.0	70.1
	JNK728	6-21	8-14	10-22	11-02	1442.2	1317.8	132.9
2023	ZD958	6-22	8-13	10-23	10-27	1399.9	1462.1	77.0
	JNK728	6-22	8-12	10-15	10-27	1375.1	1381.6	182.3

2.3. Kernel Moisture (KM)

The growth stage of each maize variety was continuously monitored and recorded. Within each plot, plants exhibiting uniform growth and pollination on the same day were selected and tagged. Sampling of maize ears began 7 days after pollination (DAP) and was conducted at 7-day intervals until the final harvest. A representative ear was collected from each plot at each sampling point. Kernels from the middle rows of each ear were manually separated, thoroughly mixed, and 100 kernels were randomly selected for fresh weight determination. The samples were then oven-dried at 105 °C for 30 min, followed by drying at 80 °C until a constant weight was achieved. The grain moisture content was calculated based on the method described by Li et al., using the following formulas [41]:

$$\text{Kernel water content (g·100 kernels)} = \text{Fresh weight (g)} - \text{dry weight (g)}$$

$$\text{Kernel moisture (\%)} = \text{Kernel water content (g)/Fresh weight (g)} \times 100\%$$

Average kernel dehydration rate before physiological maturity = (90%-kernel moisture at physiological maturity (%))/days from pollination to physiological maturity (d)

Average grain dehydration rate after physiological maturity (% d^{-1}) = (kernel moisture at physiological maturity (%)-kernel moisture at harvest (%))/days after physiological maturity (d)

Total kernel dehydration rate (% d^{-1}) = (90%-kernel moisture at harvest (%))/days from pollination to harvest

2.4. Starch Content

Maize kernels at physiological maturity were ground into fine flour and analyzed for total starch content (TS) and Amylose content (AM) of the flour by Starch and Amylose content Kit (G0507F and G0508F, Grace Biotechnology, Suzhou, China).

Amylopectin content (AP) = total starch content (TS) − Amylose content (AM)

2.5. Weight of Grain Structural Components

Maize kernels from the middle portion of the ear at physiological maturity were collected, thoroughly mixed, and soaked in distilled water overnight. The pericarp and embryo were carefully separated using tweezers. The endosperm was then sectioned using

a knife to isolate the floury and vitreous endosperm components. All separated structures were placed in aluminum boxes, oven-dried, and weighed. The weight proportion of each kernel component was subsequently calculated.

2.6. Kernel Starch Microstructure

The kernels 35 DAP and the physiological maturity were collected. Transverse sections of the kernels were excised and immediately fixed in 2.5% glutaraldehyde solution. The fixed samples were then dehydrated using a graded ethanol series (50%, 70%, 90%, and 100%), with each concentration applied in triplicate rinses. As shown in Figure 1, tissue blocks with a thickness of 2–3 mm were air-dried, sputter-coated with gold, and examined by scanning electron microscopy (SEM; Hitachi S-3400N, Hitachi, Japan). The size, shape, arrangement, and distribution of starch granules in both vitreous and floury endosperm were recorded using micrographs.

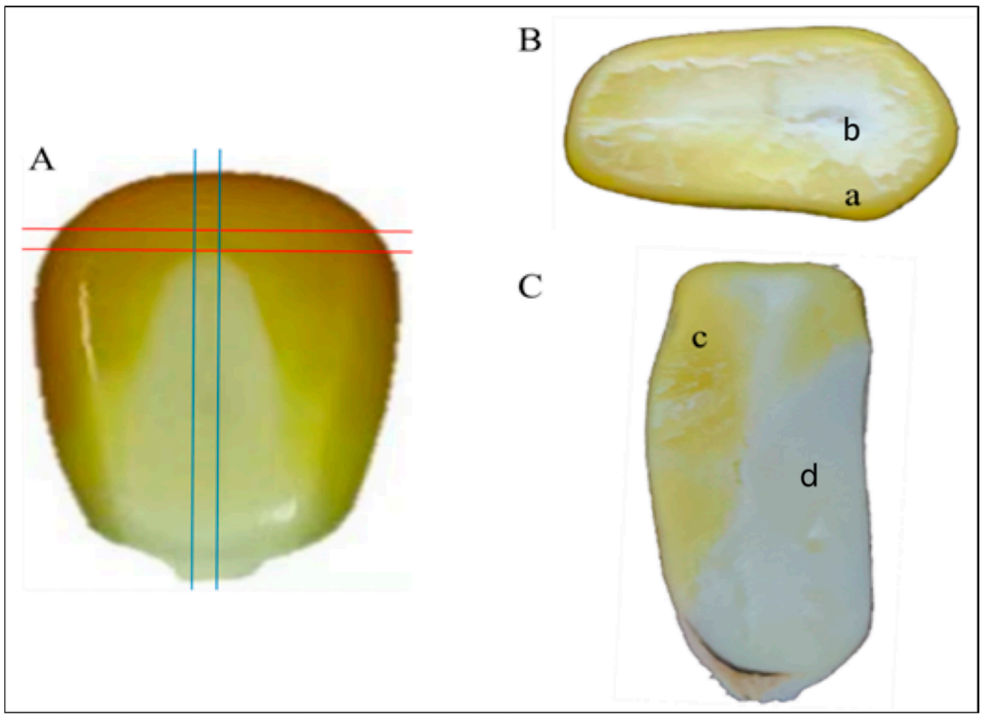

Figure 1. Schematic diagram of endosperm sampling position of transverse (**B**) and longitudinal (**C**) slices of maize kernel (**A**). Note: Vitreous endosperm sampling points of a and c; floury endosperm sampling points of b and d. The red and blue lines in (**A**) mark the transverse and longitudinal cutting positions, respectively.

2.7. Starch Granules

A total of 80 g of maize kernel at physiological maturity was used for starch extraction. The volume, number, and surface area distributions of starch granules were determined using dynamic light scattering (DLS) with a Mastersizer 3000 laser diffraction particle size analyzer (Malvern Instruments Ltd., Worcestershire, UK).

2.8. Statistical Analysis

Data recording and processing were performed using Excel 2016 (Microsoft Corp., Redmond, WA, USA). Statistical analyses of kernel dehydration parameters, kernel component proportions, and starch granule characteristics were conducted using Duncan's multiple range test at $p < 0.05$ level with SPSS 19.0 (SPSS Inc., Chicago, IL, USA). Prior to multiple

comparisons, tests for normality and homogeneity of variance were performed. SigmaPlot 12.5 software (Systat Software, San Jose, CA, USA) was applied for generating figures.

3. Results

3.1. Kernels Moisture Rate

The kernel moisture rate (KMR) of both maize varieties exhibited a monotonically decreasing trend with increasing DAP (Figure 2). Throughout the grain-filling stage, JNK728 consistently maintained a lower KMR than ZD958. The inter-varietal difference in KMR remained relatively stable during the early stages of grain development but increased significantly after 42 DAP. At physiological maturity, KMR was 25.27% for JNK728 and 28.63% for ZD958. Additionally, JNK728 reached physiological maturity earlier than ZD958. During the harvest period, the average KMR of JNK728 was 21.61% lower than that of ZD958 in both years. These results indicated that JNK728 exhibited a faster rate of physical dehydration during the late grain-filling stage and could achieve the target moisture threshold (<25%) required for mechanical grain harvesting.

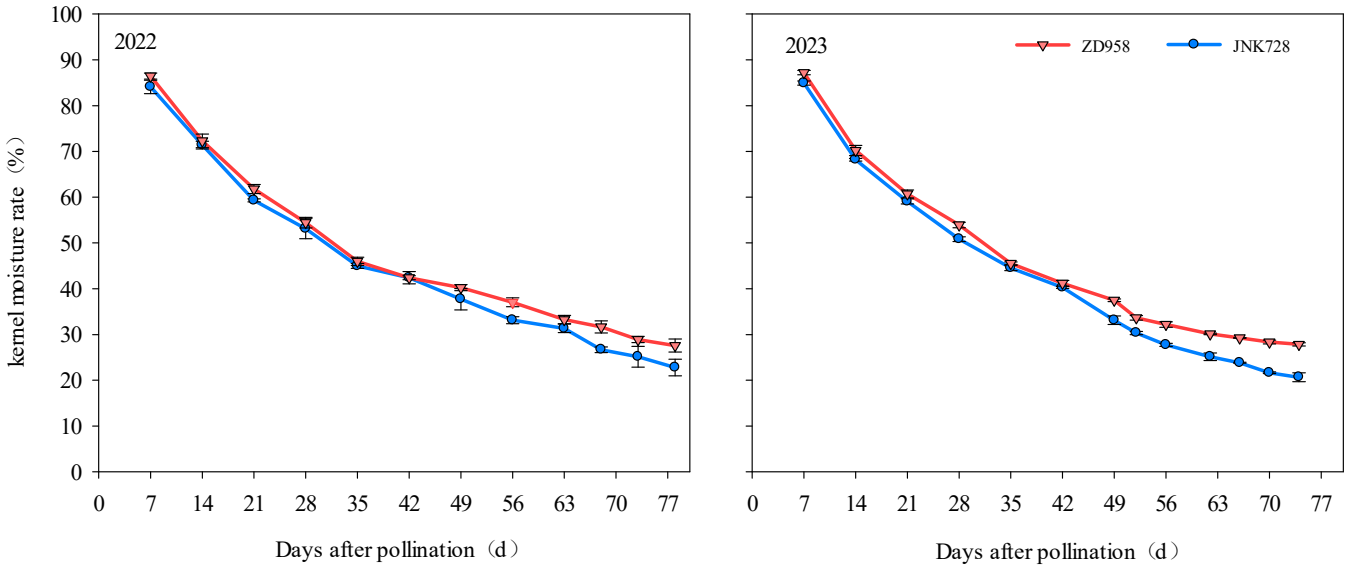

Figure 2. Kernel moisture rates of different maize varieties. Note: The kernel moisture rate in the figure is the data per 100 grains. Zhengdan958 (ZD958) is as a slow-dehydrating variety and Jingnongke (JNK728) is as a fast-dehydrating variety.

3.2. Kernel Dehydration Parameters

Significant differences in kernel dehydration parameters were observed between the two maize varieties (Figure 3). On average, the kernel dehydration rate after physiological maturity was lower than that before physiological maturity. Across both years, the pre-physiological maturity dehydration rate (pre-KDR) of ZD958 was significantly lower than that of JNK728 by 10.12% in 2022 and 15.95% in 2023. Similarly, the post-physiological maturity dehydration rate (post-KDR) of ZD958 was lower by 20.21% and 75.57% in 2022 and 2023, respectively. Over the entire dehydration period, the average dehydration rates of ZD958 were 6.33% and 10.30% lower than those of JNK728 in 2022 and 2023, respectively.

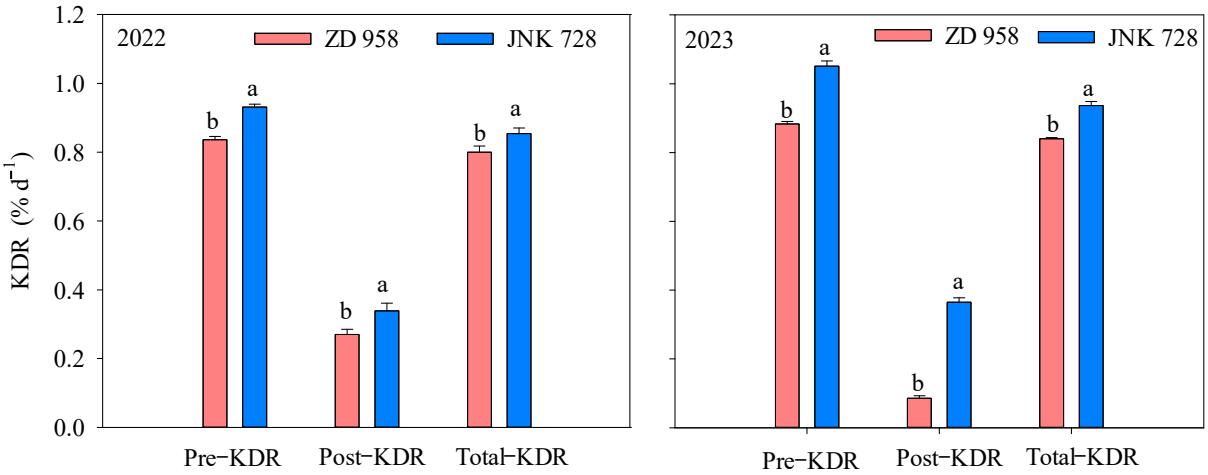

Figure 3. Kernel dehydration parameters of different maize varieties. Note: Pre-KDR is the average dehydration rate before physiological maturity. Post-KDR is the average dehydration rate after physiological maturity. Total-KDR is the total dehydration rate. Different lowercase letters indicate significant differences between varieties in different years at a significance level of 0.05.

3.3. Starch Content of Kernel

The total starch and amylopectin contents showed significant differences between the two varieties over both years (Figure 4). JNK728 exhibited larger increases than ZD958, with average increases of 6.57% in total starch and 9.89% in amylopectin content in two years. However, there was no significant difference in amylose content between the two varieties. The results indicated that the higher amylopectin content in JNK728 might contribute to its faster kernel dehydration rate.

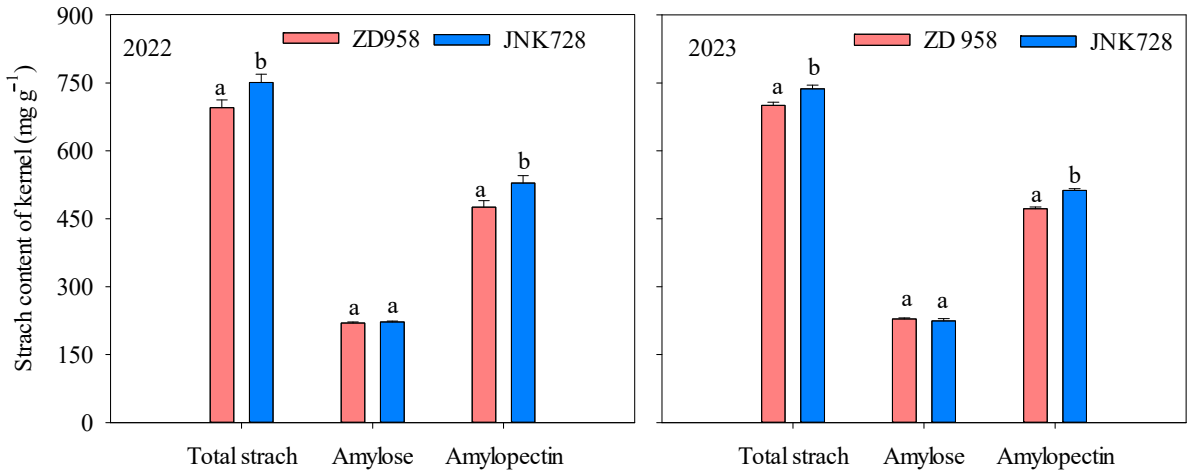

Figure 4. The content of total starch, amylose, and amylopectin in kernels of different varieties. Different lowercase letters indicate significant differences between varieties in different years at a significance level of 0.05.

3.4. Proportion of Kernel Structure Weight

As shown in Table 3, significant differences in the proportional weight of grain structural components were observed between the two maize varieties. Over the two-year period, the average pericarp weight proportion of JNK728 was significantly higher than that of ZD958 by 16.99%. The proportion of floury endosperm was also greater in JNK728, with ZD958 showing a significant 23.69% reduction compared to JNK728. In contrast, the vitreous endosperm proportion was higher in ZD958, exceeding that of JNK728 by 17.52%. Furthermore, the ratio of vitreous to floury endosperm and vitreousness was consistently

the highest in ZD958, with average increases of 52.48% and 15.64%, respectively, across both years.

Table 3. Proportion of kernel components of different maize varieties.

Year	Varieties	Pericarp (%)	Embryo (%)	Floury Endosperm (%)	Vitreous Endosperm (%)	Vitreous Endosperm/ Floury Endosperm	Vitreousness (%)
2022	ZD958	5.40 b	10.19 a	24.93 b	59.48 a	2.39 a	70.46 a
	JNK728	6.18 a	10.98 a	34.40 a	48.44 b	1.41 b	58.47 b
2023	ZD958	5.02 b	11.03 a	23.88 b	60.07 a	2.52 a	71.55 a
	JNK728	6.01 a	11.14 a	29.56 a	53.29 b	1.81 b	64.33 b

Note: Different lowercase letters indicate significant differences between varieties in different years at a significance level of 0.05.

3.5. Kernel Pericarp Structure

Distinct differences in both transverse and longitudinal sections of the pericarp were observed between the two maize varieties (Figure 5). At 35 DAP, ZD958 exhibited a thicker pericarp (42.0 μm) with fewer compartments and smaller intercellular gaps (Figure 5b), whereas JNK728 displayed a thinner and denser pericarp structure (Figure 5a,e). At physiological maturity, the pericarp of JNK728 became thicker and contained more compartments with larger gaps than its structure at 35 DAP (Figure 5c,g). The pericarp thickness of JNK728 at maturity was 52.96% greater than that of ZD958, whereas that of ZD958 remained structurally dense (Figure 5d).

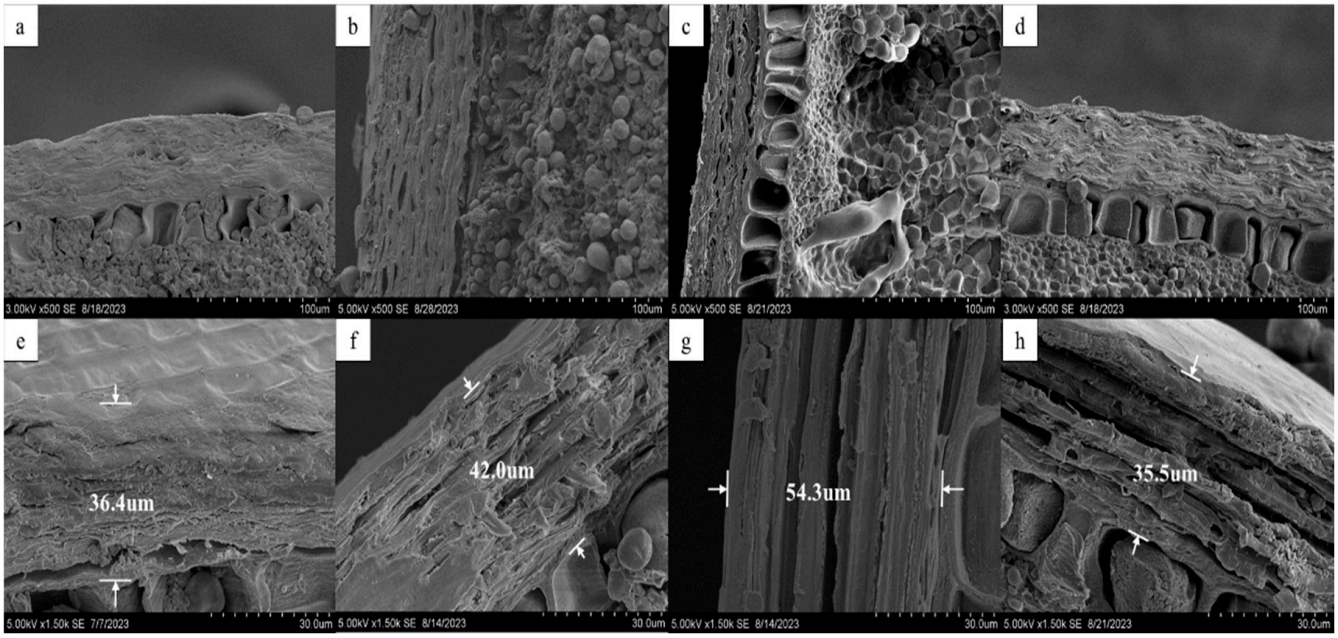

Figure 5. Horizontal and longitudinal sections of pericarp structure in different maize varieties. Note: (**a**–**d**) Pericarp structure in the horizontal section; (**e**–**h**) pericarp structure in the longitudinal section. (**a**,**b**) and (**e**,**f**) correspond to grain samples at 35 DAP, and (**c**,**d**,**g**,**h**) correspond to grain samples at maturity; (**a**,**c**,**e**,**g**) pericarp structure of JNK728; (**b**,**d**,**f**,**h**) pericarp structure of ZD958.

3.6. Microstructure Horizontal Section Endosperm Structure

As shown in Figure 6, evident differences were observed in the horizontal section of kernel endosperm structure between the two maize varieties. At 35 DAP, the starch

granules in the floury endosperm of JNK728 (Figure 6a) were predominantly spherical with smooth surfaces and a uniform size distribution. In contrast, the starch granules in ZD958 (Figure 6b) exhibited greater morphological variation, consisting mainly of spherical and polyhedral shapes. In the vitreous endosperm, both varieties showed a more compact arrangement of starch granules than their floury regions, with irregular and polyhedral structures. In JNK728, starch granules were loosely arranged and connected by matrix proteins, whereas in ZD958, the granules were densely packed and embedded within matrix proteins. At physiological maturity, no notable changes were observed in the floury endosperm of either variety, and starch granules remained predominantly spherical. However, the granule size in JNK728 (Figure 6c) was more uniform and consistent than that in ZD958 (Figure 6d). In the vitreous endosperm, JNK728 (Figure 6g) exhibited a more uniform granule size and arrangement, whereas ZD958 (Figure 6h) displayed a higher density of surface-bound matrix proteins on starch granules.

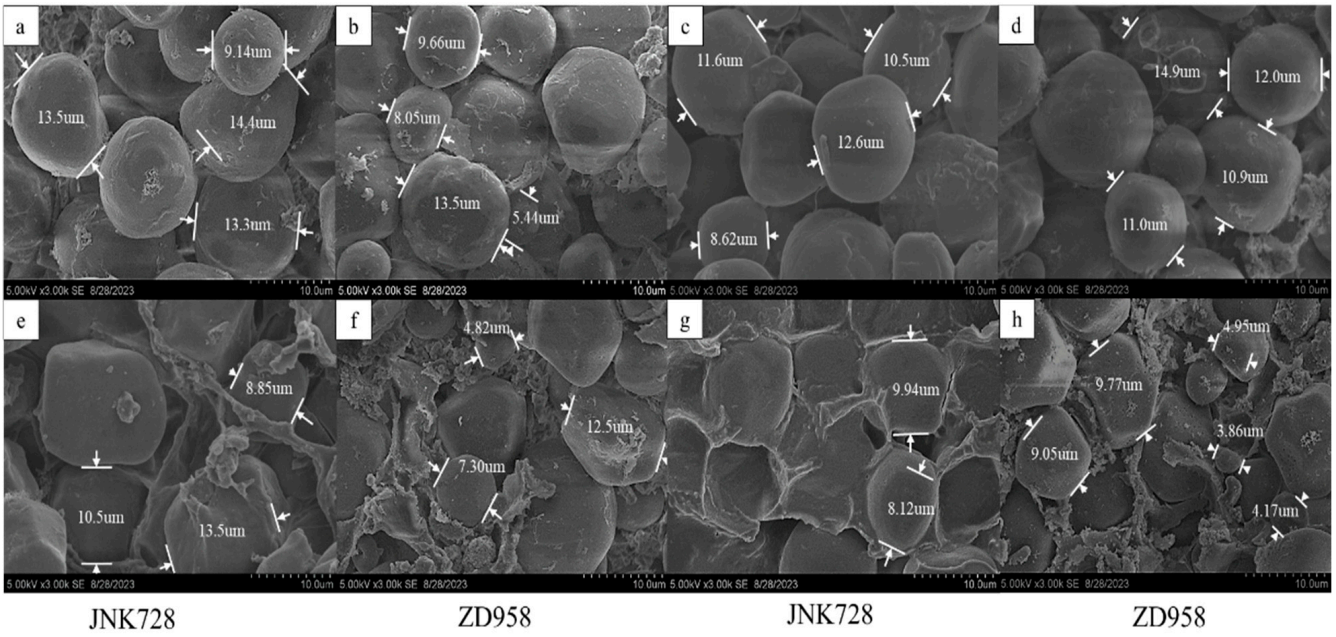

Figure 6. Transverse structure of endosperm in different varieties of grains. Note: (**a**–**d**) Floury endosperm; (**e**–**h**) vitreous endosperm. (**a**,**b**,**e**,**f**) represent grain samples at 35 DAP, and (**c**,**d**,**g**,**h**) represent grain samples at maturity. The same labeling applies to subsequent figures.

3.7. Kernel Longitudinal Section Endosperm Structure

At 35 DAP, the starch granules in the floury endosperm of JNK728 (Figure 7a) were predominantly spherical, with slightly concave surfaces and loose arrangements, and exhibited a simple intergranular structure. In contrast, ZD958 granules (Figure 7b) were uneven in size, densely packed, and rich in intergranular inclusions. In both varieties, granules in the vitreous endosperm were more tightly arranged than in the floury region. In JNK728 (Figure 7e), the granules were mainly spherical or polyhedral with smooth edges and corners. In ZD958, granules were mostly polyhedral, with distinct edges and corners, and were embedded within matrix proteins (Figure 7f).

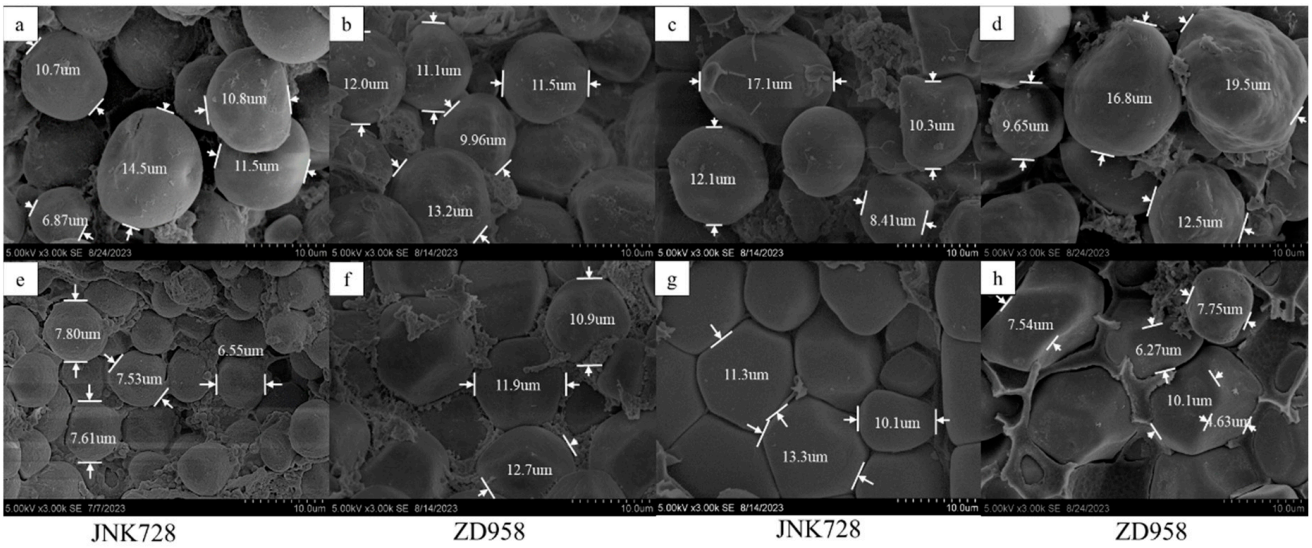

Figure 7. Vertical cutting structure of endosperm in different varieties of grains. Note: (**a**–**d**) Floury endosperm; (**e**–**h**) vitreous endosperm. (**a**,**b**,**e**,**f**) represent grain samples at 35 DAP, and (**c**,**d**,**g**,**h**) represent grain samples at maturity. The same labeling applies to subsequent figures.

At physiological maturity, starch granules in the vitreous endosperm of both varieties were denser than those at 35 DAP. In JNK728 (Figure 7c), the granules were mostly spherical with irregular shapes, variable sizes, and a loose arrangement. In ZD958 (Figure 7d), the granules were approximately spherical with uneven surfaces and non-uniform size distribution. The granule arrangement in the vitreous endosperm of ZD958 (Figure 7h) was denser than that of JNK728, with more matrix proteins observed on the granule surfaces (Figure 7g). These structural features of JNK728 may facilitate the faster kernel dehydration by promoting moisture loss.

3.8. Characteristics of Starch Granules

Tables 4–6 presented the differences in starch granule size distribution between the two varieties. Starch granules were categorized into large (≥10 μm) and small (<10 μm) particles based on their diameter. Compared to JNK728, the volume, number, and surface area proportions of large granules in ZD958 were reduced by 2.83%, 9.86%, and 4.72%, respectively, while those of small granules increased by 29.05%, 22.30%, and 27.48%.

In 2022, the peak diameter of the starch granule volume in ZD958 was 5.49% smaller than that in JNK728, and similar results were observed in 2023 (Table 4). The peak diameter for granule number was identical between the two varieties in both years (Table 5). The surface area peak diameters of JNK728 were 6.62% and 14.17% higher than those of ZD958 in 2022 and 2023, respectively (Table 6).

Table 4. Volume distribution of starch granules in different varieties.

Year	Hybrids	Diameter of Starch Granule (%)		D (4,3)	Peak Diameter (μm)
		<10 μm	≥10 μm	(μm)	
2022	ZD958	12.29 a	87.92 b	17.23	15.5
	JNK728	9.13 b	90.88 a	17.07	16.4
2023	ZD958	11.41 a	88.58 b	15.90	14.5
	JNK728	9.24 b	90.76 a	16.80	14.5

Note: D (4,3) indicates volume-weighted average. Different lowercase letters indicate significant differences between varieties in different years at a significance level of 0.05.

Table 5. Number distribution of starch granules in different varieties.

Year	Hybrids	Diameter of Starch Granule (%)		D (1,0)	Peak Diameter (μm)
		<10 μm	≥10 μm	(μm)	
2022	ZD958	40.98 a	59.01 b	12.80	11.2
	JNK728	30.92 b	69.07 a	13.47	11.2
2023	ZD958	34.05 a	65.95 b	13.00	11.2
	JNK728	30.43 b	69.56 a	13.43	11.2

Note: D (1,0) indicates number-weighted average. Different lowercase letters indicate significant differences between varieties in different years at a significance level of 0.05.

Table 6. Surface area distribution of starch granules in different varieties.

Year	Hybrids	Diameter of Starch Granule (%)		D (3,2)	Peak Diameter (μm)
		<10 μm	≥10 μm	(μm)	
2022	ZD958	19.98 a	80.02 b	15.60	13.6
	JNK728	14.67 b	85.32 a	15.77	14.5
2023	ZD958	17.41 a	82.59 b	14.90	12.7
	JNK728	14.66 b	85.34 a	15.60	14.5

Note: D (3,2) indicates the surface area-weighted average. Different lowercase letters indicate significant differences between varieties in different years at a significance level of 0.05.

3.9. Correlation Analysis

Correlation analysis revealed that kernel dehydration rate was significantly associated with both structural component proportions and starch granule characteristics (Figure 8). The total kernel dehydration rate (T-KDR) showed strong positive correlations with Pre-KDR (r = 0.99 ***) and Post-KDR (r = 0.96 ***), while Pre-KDR was also positively correlated with Post-KDR (r = 0.96 ***). Both Pre- and Post-KDR were positively correlated with TS, AP, PSC, PFE, B-SASG, B-VSG, and B-NSG but negatively correlated with PVE, VE/FE, V, S-SASG, S-VSG, and S-NSG.

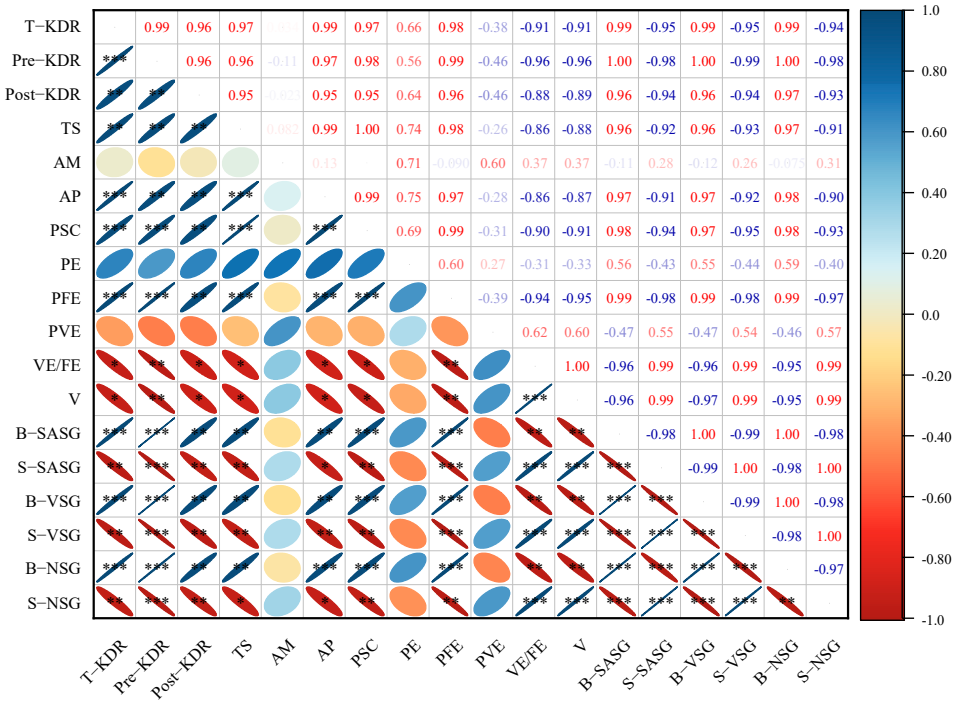

Figure 8. Correlation analysis between different parameters. Note: Pre-KDR: average dehydration rate before physiological maturity; Post-KDR: average dehydration rate after physiological maturity;

T-KDR: total dehydration rate; TS: total starch content; AM: Amylose content; AP: Amylopectin content; PSC: proportion of pericarp weight; PE: proportion of embryo weight; PFE: proportion of floury endosperm weight; PVE: proportion of vitreous endosperm weight; VE/FE: ratio of honey endosperm weight to floury endosperm weight; V: vitreousness; B-SASG: surface area distribution of large starch granules; S-SASG: surface area distribution of small starch granules; B-VSG: volume distribution of large starch granules; S-VSG: volume distribution of small starch granules; B-NSG: number distribution of large starch granules; S-NSG: number distribution of small starch granules. Significance levels: * $p \leq 0.05$, ** $p \leq 0.01$, *** $p \leq 0.001$.

4. Discussion

High kernel moisture content at harvest is unsuitable for mechanical grain harvesting [42] and remains a major constraint limiting its large-scale adoption [43]. Previous studies have suggested that the optimal kernel moisture content for high-quality mechanical grain harvesting ranges from 15% to 25% [10]. In this study, the kernel moisture content at physiological maturity for JNK728 and ZD958 was 26.69% and 28.91% (2022), and 23.84% and 27.59% (2023), respectively. At harvest, the values were 23.38% and 27.59% (2022) and 20.66% and 27.84% (2023), respectively, indicating that JNK728 can meet the moisture threshold required for mechanical harvesting. Kernel dehydration was divided into two stages. The first stage represents a developmental dehydration phase related to grain filling that lasts until physiological maturity. The second is a physical dehydration phase that occurs after maturity [18]. Final kernel moisture can be influenced by moisture at physiological maturity and the post-maturity dehydration rate [44]. In our study, the varieties with lower harvest moisture exhibited higher Pre-KDR and Post-KDR. Wang et al. (2023) reported that the cultivars with longer post-anthesis durations, such as ZD958, were less suitable for mechanical grain harvest [6]. Consistently, ZD958 required more thermal time for milk line disappearance than JNK728, with increases of 2.52% (2022) and 5.83% (2023).

As the outer protective tissue of the maize kernel, the pericarp supports and shields the embryo and endosperm from mechanical damage and pest invasion [45] and plays a key role in regulating the kernel dehydration rate [46]. Previous studies have shown that pericarp thickness can be associated with seed maturity and moisture content [47], and that thinner, more permeable pericarp facilitate dehydration [33]. Gong et al. (2024) reported that pericarp thickness increased during early development, reached a maximum, and then decreased toward maturity [48]. Our findings indicated that at 35 DAP, ZD958 had a pericarp 5.6 μm thicker than JNK728, with fewer cavities and smaller gaps. At physiological maturity, the pericarp of ZD958 became thinner and more compact, whereas that of JNK728 exhibited larger cavities and gaps than 35 DAP. These structural characteristics, including thin pericarp and expanded gaps, may contribute to the enhanced dehydration efficiency observed in JNK728.

Maize endosperm is classified as vitreous and floury types. Starch exists in granular form within the endosperm [37,49], and its physicochemical properties are influenced by the starch granule size distribution. Prior studies showed that vitreous endosperm had a hard, compact texture, whereas the floury endosperm was soft and loosely structured [50]. Starch granules in the vitreous endosperm were polygonal, tightly packed, and contain minimal air spaces, whereas those in the floury endosperm were mostly spherical, loosely packed, and interspersed with extensive air voids [39,51]. In the vitreous endosperm, the granules were embedded within a dense, continuous protein matrix, which was sparse or absent in the floury endosperm [40,52]. In maize, starch granules were closely associated with proteins, particularly in the endosperm. The distinction between vitreous and floury endosperm was primarily determined by the presence and density of the protein matrix, with vitreous endosperm containing significantly more starch-associated proteins [37],

resulting in a more compact texture. Additionally, vitreous endosperm had been reported to possess a higher amylose content [36]. Our results were consistent with those of previous studies (Figures 6 and 7). Microstructural analysis revealed clear differences in the endosperm composition between JNK728 and ZD958. The floury endosperm of JNK728 exhibited more uniformly sized starch granules with smooth surfaces, larger intergranular air spaces, and a loosely packed arrangement than those of ZD958. In the vitreous endosperm, JNK728 showed spherical and polyhedral granules with rounded edges, whereas ZD958 predominantly featured polyhedral granules with sharply defined edges embedded or fully encapsulated in matrix proteins. We propose that this microstructure of JNK728 creates extensive and interconnected air voids to facilitate the outward diffusion and evaporation of moisture from the kernel. As a key indicator of endosperm texture, vitreousness is defined as the dry weight percentage of vitreous endosperm relative to the total endosperm mass [53]. Higher vitreousness corresponds to a greater proportion of vitreous endosperm and denser starch packing. Our results showed that ZD958 exhibited the highest vitreousness over two consecutive years, while JNK728 demonstrated an average reduction of 8.90% compared to ZD958. In both varieties, vitreous endosperm weight exceeded that of floury endosperm. However, JNK728, characterized by faster dehydration, had a higher proportion of floury endosperm, whereas ZD958, with slower dehydration, had a greater proportion and higher ratio of vitreous to floury endosperm. These differences suggested that greater vitreousness and a higher vitreous-to-floury endosperm ratio contribute to the slower dehydration of ZD958. Conversely, the enhanced dehydration rate of JNK728 may be attributed to its predominance of floury endosperm, smooth-surfaced granules, expanded intergranular spaces, and loosely packed endosperm architecture, enhancing water vapor escape. Therefore, endosperm structural heterogeneity may play a critical role in the regulation of kernel dehydration dynamics.

Starch in the maize endosperm exists in granular form, and the size and distribution of starch granules are the key determinants of kernel quality [34]. Previous studies had classified maize starch granules differently. Lu et al. identified the small (<3 μm), medium (3–17 μm), and large (>17 μm) granules, while Paterson et al. reported a typical size range of 7–25 μm with an average diameter of 10 μm [54,55]. Rubí et al. defined granules ≥10 μm as large and those <10 μm as small [56]. Such inconsistencies in classification may arise from differences in starch isolation methods and particle size measurement techniques [57]. In this study, a 10 μm threshold was adopted to classify the starch granules into large (≥10 μm) and small (<10 μm) categories. The average proportions of large and small starch granules in terms of volume, number, and surface area, were 88.25–90.82% vs. 9.19–11.85%, 62.48–69.32% vs. 30.68–37.52%, and 81.31–85.33% vs. 14.67–18.70%, respectively, indicating a predominance of large granules in maize kernels. The volume, number, and surface area distribution of large granules (≥10 μm) were significantly higher in JNK728 than in ZD958. Previous studies had shown that small granules contribute less to the total starch content [58], and a greater volumetric proportion of large granules was positively associated with total starch accumulation [59]. Consistent with these findings, our results revealed that JNK728, a fast-dehydrating variety, exhibited a 2.91% higher volumetric proportion of large granules and 6.57% greater total starch content than ZD958 ($p < 0.05$). Correlation analysis revealed that the volume, number, and surface area of large starch granules were highly significantly and positively correlated with both the kernel dehydration rate and the proportion of floury endosperm.

The kernel dehydration process is markedly modulated by genotype-by-environment interactions. Thus, the applicability of the study's conclusions to varying ecological contexts further investigation. Furthermore, our microstructural observations implicate kernel microstructure and starch granule arrangement are the primary causes of differential

dehydration rates. Nevertheless, the intrinsic physiological basis, particularly the molecular mechanisms governing starch synthesis, has yet to be determined.

5. Conclusions

Comparative analysis revealed that JNK728 exhibited a 9.12% higher total kernel dehydration rate than ZD958 ($p < 0.01$), and this advantage was consistently evident during the pre- and post-physiological maturity phase. Moreover, a higher content of amylopectin in the kernels contributed to its rapid dehydration. Our results indicated that fast-dehydrating maize varieties possess distinct structural features: lower vitreousness, reduced vitreous-to-floury endosperm ratio, higher proportion of large starch granules (≥10 μm), smooth surfaces, uniform sizes, and loosely packed arrangements. These findings enhance our understanding of the relationship between kernel dehydration dynamics, microstructural traits, and starch granule size distribution, and provide a theoretical basis for selecting maize varieties that are better suited for efficient mechanized grain harvesting.

Author Contributions: Conceptualization, X.S., W.J. and Q.S.; methodology, X.S., X.L., F.S., Z.L., Y.Y., X.H., L.L., Z.W., Z.S. and J.L.; software, X.L. and F.S.; formal analysis, X.L., F.S., Z.L., Y.Y., X.H., L.L., Z.W., Z.S. and J.L.; investigation, X.L., X.H., L.L., Z.W., Z.S. and J.L.; data curation, X.L.; writing—original draft preparation, X.L. and X.S.; writing—review and editing, X.S., W.J. and Q.S.; visualization, X.L.; supervision, X.S.; funding acquisition, X.S. and W.J. All authors have read and agreed to the published version of the manuscript.

Funding: This research was funded by the National Natural Science Foundation of China, grant number 32201906; the Shandong Agriculture Research System, grant number SDARS-02-06; Qingdao Agricultural University High-level Talents Research Foundation, grant number 663/1119019; and the Natural Science Foundation Project of Inner Mongolia Autonomous Region, grant number 2023QN03013.

Institutional Review Board Statement: Not applicable.

Data Availability Statement: The original contributions presented in this study are included in the article. Further inquiries can be directed to the corresponding author.

Conflicts of Interest: The authors declare no conflicts of interest.

References

1. Luo, N.; Meng, Q.F.; Feng, P.Y.; Qu, Z.R.; Yu, Y.H.; Liu, D.L.; Muller, C.; Wang, P. China can be self-sufficient in maize production by 2030 with optimal crop management. *Nat. Commun.* **2023**, *14*, 2637. [CrossRef]
2. FAO. Statistics for Trade of Crops and Livestock Products-Dataset. 2021. Available online: https://www.fao.org/faostat/en/#data/QCL (accessed on 14 October 2025).
3. Xie, R.Z.; Ming, B.; Gao, S.; Wang, K.R.; Hou, P.; Li, S.K. Current state and suggestions for mechanical harvesting of corn in China. *J. Integr. Agric.* **2022**, *21*, 892–897. [CrossRef]
4. MARAC (Ministry of Agriculture and Rural Affairs of China). Online Statistical Database: Agricultural Machinery. 2016. Available online: http://zdscxx.moa.gov.cn:8080/nyb/pc/frequency.jsp# (accessed on 10 March 2020).
5. Li, S.K.; Wang, K.R.; Xie, R.Z.; Ming, B. Grain mechanical harvesting technology promotes the transformation of maize production mode. *Sci. Agric. Sin.* **2018**, *51*, 1842–1844.
6. Wang, J.T.; Dong, X.L.; Qiu, R.J.; Lou, B.Y.; Tian, L.; Chen, P.; Zhang, X.J.; Liu, X.J.; Sun, H.Y. Optimization of sowing date and irrigation schedule of maize in different cropping systems by APSIM for realizing grain mechanical harvesting in the North China Plain. *Agric. Water Manag.* **2023**, *276*, 108068. [CrossRef]
7. Wang, X.Y.; Tan, W.M.; Zhou, S.L.; Xu, Y.; Cui, T.; Gao, H.; Chen, M.L.; Dong, X.H.; Sun, H.Y.; Yang, J.Z.; et al. Converting maize production with low emergy cost and high economic return for sustainable development. *Renew Sustain. Energy Rev.* **2021**, *136*, 110443. [CrossRef]
8. Shi, W.J.; Shao, H.; Sha, Y.; Shi, R.; Shi, D.F.; Chen, Y.C.; Ban, X.B.; Mi, G.H. Grain dehydration rate is related to post-silking thermal time and ear characters in different maize hybrids. *J. Integr. Agric.* **2022**, *21*, 964–976. [CrossRef]
9. Wang, K.R.; Li, S.K. Analysis of influencing factors on kernel dehydration rate of maize hybrids. *Sci. Agric. Sin.* **2017**, *50*, 2027–2035. [CrossRef]

10. Wang, X.Y.; Wang, X.L.; Xu, C.C.; Tan, W.M.; Wang, P.; Meng, Q.F. Decreased kernel moisture in medium-maturing maize hybrids with high yield for mechanized grain harvest. *Crop Sci.* **2019**, *59*, 2794–2805. [CrossRef]
11. Wang, J.T.; Dong, X.L.; Xiao, Y.; Liu, Q.S.; Zhang, D.M.; Han, J.L.; Liu, Y.; Gao, G.R.; Liu, Z.M.; Sun, H.Y. Analysis of kernel dry down process after physiological maturity of spring maize based on diffusion theory in the North China. *Chin. J. Eco-Agric.* **2020**, *28*, 545–557. [CrossRef]
12. Chai, Z.W.; Wang, K.R.; Guo, Y.Q.; Xie, R.Z.; Li, L.L.; Ming, B.; Hou, P.; Liu, C.W.; Chu, Z.D.; Zhang, W.X.; et al. Current status of maize mechanical grain harvesting and its relationship with grain moisture content. *Sci. Agric. Sin.* **2017**, *50*, 2036–2043. [CrossRef]
13. Yin, S.Y.; Liu, J.; Yang, T.T.; Li, P.C.; Xu, Y.; Fang, H.M.; Xu, S.H.; Wei, J.; Xue, L.; Hao, D.R.; et al. Genetic analysis of the seed dehydration process in maize based on a logistic model. *Crop J.* **2020**, *8*, 182–193. [CrossRef]
14. Liu, J.J.; Yu, H.; Liu, Y.L.; Deng, S.N.; Liu, Q.C.; Liu, B.S.; Xu, M.L. Genetic dissection of grain water content and dehydration rate related to mechanical harvest in maize. *BMC Plant Biol.* **2020**, *20*, 118. [CrossRef] [PubMed]
15. Yu, Y.H.; Li, W.Q.; Liu, Y.F.; Liu, Y.J.; Zhang, Q.Z.; Ouyang, Y.D.; Ding, W.Y.; Xue, Y.; Zou, Y.L.; Yan, J.H.; et al. A Zea genus-specific micropeptide controls kernel dehydration in maize. *Cell* **2025**, *188*, 44–59.e21. [CrossRef] [PubMed]
16. Plett, S. Corn kernel breakage as a function of grain moisture at harvest in a prairie environment. *Can. J. Plant Sci.* **1994**, *74*, 543–544. [CrossRef]
17. Dai, L.Q.; Wu, L.; Dong, Q.S.; Zhang, Z.; Wu, N.; Song, Y.; Lu, S.; Wang, P.W. Genome-wide association study of field grain drying rate after physiological maturity based on a resequencing approach in elite maize germplasm. *Euphytica* **2017**, *213*, 182. [CrossRef]
18. Brooking, I.R. Maize ear moisture during grain-filling, and its relation to physiological maturity and grain-drying. *Field Crops Res.* **1990**, *23*, 55–68. [CrossRef]
19. Nielsen, R.L. *Field Dry Down of Mature Corn Grain*; Purdue University: West Lafayette, IN, USA, 2005; Available online: http://www.kingcorn.org/news/articles.05/GrainDrying-0815.html (accessed on 14 October 2025).
20. Wan, Z.H.; Ren, B.Z.; Zhao, B.; Liu, P.; Dong, S.T.; Zhang, J.W. Grain filling and dehydration characteristics of summer maize hybrids differing in maturities and effect of plant density. *Acta Agron. Sin.* **2018**, *44*, 1517–1526. [CrossRef]
21. Yang, J.; Carena, M.J.; Uphaus, J. Area under the dry down curve (AUDDC): A method to evaluate rate of dry down in maize. *Crop Sci.* **2010**, *50*, 2347–2354. [CrossRef]
22. Zhou, G.F.; Hao, D.R.; Xue, L.; Chen, G.Q.; Lu, H.H.; Zhang, Z.L.; Shi, M.L.; Huang, X.L.; Mao, Y.X. Genome-wide association study of kernel moisture content at harvest stage in maize. *Breed. Sci.* **2018**, *68*, 622–628. [CrossRef]
23. Hicks, D.R.; Geadelmann, G.L.; Peterson, R.H. Drying rates of frosted maturing maize. *Agron. J.* **1976**, *68*, 452–455. [CrossRef]
24. Li, L.L.; Gu, W.R.; Zuo, S.Y.; Meng, Y.; Li, C.F.; Li, W.H.; Zhang, Z.Y.; Wei, S. Effects of thidiazuron and ethephon on the grain filling and dehydration characteristics of maize in Northeast China. *Arch. Agron. Soil Sci.* **2020**, *68*, 886–902. [CrossRef]
25. Cavalieri, A.J.; Smith, O.S. Grain filling and field drying of a set of maize hybrids released from 1930 to 1982. *Crop Sci.* **1985**, *25*, 856–860. [CrossRef]
26. Crane, P.L.; Miles, S.R.; Newman, J.E. Factors associated with varietal differences in rate of field drying in corn. *Agron. J.* **1959**, *51*, 318–320. [CrossRef]
27. Mathre, D.E.; Johnston, R.H.; Martin, J.M. Sources of resistance to *Cephalosporium gramineum* in *Triticum* and *Agropyron* species. *Euphytica* **1985**, *34*, 419–424. [CrossRef]
28. Pineda-Gomez, P.; Rosales-Rivera, A.; Gutierrez-Cortez, E.; Rodriguez-Garcia, M.E. Comparative analysis of the water diffusion in the corn grains, with and without pericarp during the thermo-alkaline treatment. *Food Bioprod. Process.* **2020**, *119*, 38–47. [CrossRef]
29. Huang, Z.F.; Li, L.L.; Hou, L.Y.; Gao, S.; Ming, B.; Xie, R.Z.; Hou, P.; Wang, K.R.; Xue, J.; Li, S.K. Accumulated temperature requirement for field stalk dehydration after maize physiological maturity in different planting regions. *Sci. Agric. Sin.* **2022**, *55*, 680–691. [CrossRef]
30. Troyer, A.F.; Ambrose, W.B. Plant characteristics affecting field drying rate of ear corn. *Crop Sci.* **1971**, *11*, 529–531. [CrossRef]
31. Qu, J.Z.; Zhong, Y.Y.; Ding, L.; Liu, X.X.; Xu, S.T.; Guo, D.W.; Blennow, A.; Xue, J.Q. Biosynthesis, structure and functionality of starch granules in maize inbred lines with different kernel dehydration rate. *Food Chem.* **2022**, *368*, 130796. [CrossRef]
32. Li, D.Z.; Wang, J.L.; Zhang, Y.; Lu, X.J.; Du, J.J.; Guo, X.Y. CT-Based Phenotyping and Genome-Wide Association Analysis of the Internal Structure and Components of Maize Kernels. *Agronomy* **2023**, *13*, 1078. [CrossRef]
33. Zhang, L.G.; Fan, Q.J.; Chen, X.C.; Li, B.; Zhang, Y.; Xiu, L.L. Correlation analysis on dry-down rate and main agricultural traits in maize after physiological maturity. *Heilongjiang Agric. Sci.* **2012**, *3*, 1–5.
34. Cui, L.N.; Dong, S.T.; Zhang, J.W.; Liu, P. Starch granule size distribution and morphogenesis in maize (*Zea mays* L.) grains with different endosperm types. *Aust. J. Crop Sci.* **2014**, *8*, 1560–1565. Available online: https://search.informit.org/doi/10.3316/informit.820885364920205 (accessed on 14 October 2025).
35. Li, W.Y.; Wu, P.J.; Zhang, D.P.; Yan, S.H. Granule size distribution and pasting properties of starch in normal, waxy and sweet maize kernels. *Bangladesh J. Bot.* **2020**, *49*, 949–956. [CrossRef]

36. Gayral, M.; Gaillard, C.; Bakan, B.; Dalgalarrondo, M.; Elmorjani, K.; Delluc, C.; Brunet, S.; Linossier, L.; Morel, M.-H.; Marion, D. Transition from vitreous to floury endosperm in maize (*Zea mays* L.) kernels is related to protein and starch gradients. *J. Cereal Sci.* **2016**, *68*, 148–154. [CrossRef]
37. Xu, A.H.; Lin, L.S.; Guo, K.; Liu, T.X.; Yin, Z.T.; Wei, C.X. Physicochemical properties of starches from vitreous and floury endosperms from the same maize kernels. *Food Chem.* **2019**, *291*, 149–156. [CrossRef] [PubMed]
38. Zhang, H.Y.; Gao, R.Q.; Dong, S.T. Anatomical and physiological characteristics associated with corn endosperm texture. *Agron. J.* **2011**, *103*, 1258–1264. [CrossRef]
39. Miao, M.; Li, R.; Jiang, B.; Cui, S.W.; Lu, K.Y.; Zhang, T. Structure and digestibility of endosperm water-soluble α-glucans from different sugary maize mutants. *Food Chem.* **2014**, *143*, 156–162. [CrossRef]
40. Watson, S.A. Structure and composition. In *Corn Chemistry and Technology*; Watson, S.A., Ramstad, P.E., Eds.; American Association of Cereal Chemists, Inc.: St. Paul, MN, USA, 1987; pp. 53–82.
41. Li, L.L.; Ming, B.; Gao, S.; Xie, R.Z.; Hou, P.; Wang, K.R.; Li, S.K. Study on grain dehydration characters of summer maize and its relationship with grain filling. *Sci. Agric. Sin.* **2018**, *51*, 1878–1889.
42. Liu, Y.L.; Li, M.M.; Liu, J.J.; Deng, S.N.; Zhang, Y.; Xia, Y.F.; Liu, B.S.; Xu, M.L. Multi-omics analysis reveals the pivotal role of phytohormone homeostasis in regulating maize grain water content. *Crop J.* **2024**, *12*, 1081–1092. [CrossRef]
43. Guo, Y.N.; Hou, L.Y.; Li, L.L.; Gao, S.; Hou, J.F.; Ming, B.; Xie, R.Z.; Xue, J.; Hou, P.; Wang, K.R.; et al. Study of corn kernel breakage susceptibility as a function of its moisture content by using a laboratory grinding method. *J. Integr. Agric.* **2022**, *21*, 70–77. [CrossRef]
44. Chase, S.S. Relation of yield and number of days from planting to flowering in early maturity maize hybrids of equivalent grain moisture at harvest. *Crop Sci.* **1964**, *4*, 111–112. [CrossRef]
45. Zhang, J.H.; Yue, Y.; Hu, M.J.; Yi, F.; Chen, J.; Lai, J.S.; Xin, B.B. Dynamic transcriptome landscape of maize pericarp development. *Plant J.* **2024**, *117*, 1574–1591. [CrossRef]
46. Hu, X.W.; Wang, Y.R.; Wu, Y.P. Effects of the pericarp on imbibition, seed germination, and seedling establishment in seeds of *Hedysarum scoparium* Fisch. et Mey. *Ecol. Res.* **2009**, *24*, 559–564. [CrossRef]
47. Helm, J.L.; Zuber, M.S. Effect of harvest date on pericarp thickness in dent corn. *Can. J. Plant Sci.* **1970**, *50*, 411–413. [CrossRef]
48. Gong, G.T.; Jia, H.T.; Tang, Y.Q.; Pei, H.; Zhai, L.H.; Huang, J. Genetic analysis and QTL mapping for pericarp thickness in maize (*Zea mays* L.). *BMC Plant Biol.* **2024**, *24*, 338. [CrossRef]
49. Huang, L.C.; Tan, H.Y.; Zhang, C.Q.; Li, Q.F.; Liu, Q.Q. Starch biosynthesis in cereal endosperms: An updated review over the last decade. *Plant Commun.* **2021**, *2*, 100237. [CrossRef]
50. Wang, D.; Eckhoff, S.R. Effect of broken corn levels on water absorption and steepwater characteristics. *Cereal Chem.* **2020**, *77*, 525–528. [CrossRef]
51. Timm, N.D.S.; Ramos, A.H.; Ferreira, C.D.; Biduski, B.; Eicholz, E.D.; Oliveira, M.D. Effects of drying temperature and genotype on morphology and technological, thermal, and pasting properties of corn starch. *Int. J. Biol. Macromol.* **2020**, *165*, 354–364. [CrossRef]
52. Dombrink-Kurtzman, M.A.; Knutson, C.A. A study of maize endosperm hardness in relation to amylose content and susceptibility to damage. *Cereal Chem.* **1997**, *74*, 776–780. [CrossRef]
53. Kljak, K.D.; Grbeša, D.; Aleuš, D. Relationships between kernel physical properties and zein content in corn hybrids. *Bull. UASVM Agric.* **2011**, *68*, 188–194. [CrossRef]
54. Lu, M.L.; Zhang, Y.T.; Ren, H.; Wang, T.J.; Han, Y.M.; Li, W.Y.; Li, C.F. Effects of increasing density on the granule size distribution and viscosity parameters of endosperm starch in spring maize kernel. *Sci. Agric. Sin.* **2023**, *56*, 1646–1657.
55. Paterson, J.L.; Hardacre, A.; Li, P.; Rao, M.A. Rheology and granule size distribution of corn starch dispersions from two genotypes and grown in four regions. *Food Hydrocoll.* **2001**, *15*, 453–459. [CrossRef]
56. Utrilla-Coello, R.G.; Agama-Acevedo, E.; Rosa, A.P.B.D.L.; Rodríguez-Ambriz, S.L.; Bello-Pérez, L.A. Physicochemical and enzyme characterization of small and large starch granules isolated from two maize cultivars. *Cereal Chem.* **2010**, *87*, 50–56. [CrossRef]
57. Park, S.H.; Wilson, J.D.; Seabourn, B.W. Starch granule size distribution of hard red winter and hard red spring wheat: Its effects on mixing and breadmaking quality. *J. Cereal Sci.* **2009**, *49*, 98–105. [CrossRef]
58. Svihus, B.; Uhlen, A.K.; Harstad, O.M. Effect of starch granule structure, associated components and processing on nutritive value of cereal starch: A review. *Anim. Feed Sci. Technol.* **2005**, *122*, 303–320. [CrossRef]
59. Shi, D.Y.; Zhang, H.Y.; Dong, S.T. Effects of supplemental irrigation and nitrogen application on starch granule size distribution of maize grain. *Sci. Agric. Sin.* **2014**, *47*, 633–643.

Disclaimer/Publisher's Note: The statements, opinions and data contained in all publications are solely those of the individual author(s) and contributor(s) and not of MDPI and/or the editor(s). MDPI and/or the editor(s) disclaim responsibility for any injury to people or property resulting from any ideas, methods, instructions or products referred to in the content.